BUILDING EXTRACTION FROM HIGH RESOLUTION COLOR IMAGERY BASED ON EDGE FLOW DRIVEN ACTIVE CONTOUR AND JSEG

Yonghak Song, Jie Shan

School of Civil Engineering, Purdue University, 1284 Civil Engineering Building, West Lafayette, IN 47906, USA – {song10, jshan}@purdue.edu

Commission III, WG III/4

KEY WORDS: Building, Extraction, Active contour, Level set method, Segmentation, Edge flow, JSEG

ABSTRACT:

Building extraction and delineation is one of the most salient problems in cartographic features extraction. This paper presents a novel framework for reliable and accurate building extraction from high-resolution color imagery focusing on building boundary delineation and building roof compositional polygon segmentation. Proposed framework consists of three steps. First, anisotropic diffusion and clustering are applied as pre-processing for denoising and color quantization and then building boundary is extracted by active contour driven by edge-flow. Finally, building roof compositional polygons are segmented by JSEG. The framework is tested on a number of buildings and the results are shown. The result shows the completeness and accuracy that this framework can provide for extracting building from a high-resolution color image data set.

1. INTRODUCTION

For decades, automatic and semiautomatic extraction of cartographic features from various data sets such as aerial image, digital surface model (DSM), or terrestrial images has become an intensive research topic to substitute the time-consuming and tedious manual digitizing. Among those features, buildings are the most salient in terms of their significance and complexity. Automatic building extraction has numerous applications is in geographic information system (GIS), cartographic analysis, urban planning, visualization, and telecommunication.

Many automatic building extraction methods from DSM or multi-spectral imagery are developed but suffer from rough delineation result due to the relatively low resolution of the involved DSM and multi-spectral imagery. Also, low resolution and deficiency of the method cause the fact that several buildings and possibly their surroundings are extracted as one building. Therefore, the results can only used as an initial approximation to the final building and must be enhanced with improved reliability and further refined for better accuracy.

This paper presents a novel framework for reliable and accurate building extraction from high resolution color imagery. It is focused on the delineation of building boundary and segmentation of building roof polygons or faces. First, the J-image (Deng et al., 1999) is generated from an initial unsupervised classification using anisotropic diffusion (Perona and Malik, 1990) and k-means clustering. After that, the building boundary is extracted by multi-scale active contour with the edge-flow (Ma and Majunath, 2000) as the underlying velocity field for deformation and the J-image as the stopping function based on the level set method (Osher and Sethian, 1988). Finally, building roof compositional polygons are segmented by JSEG (Deng et al., 1999). This paper will present technical details of the proposed approach by providing step by step intermediate results. The results demonstrate that the extracted building boundary coincides with the building image well and the segmented building roof polygons are close in shape to the real building roofs.

The rest of this paper is organized as follows. Section 2 briefs the previous work for automatic and semi-automatic building extraction. Section 3 explains the proposed methodology and describes the detail process. Section 4 presents our implementation and shows its results on a real scene. The paper concludes on its performance and potentials, and future prospects in section 5.

2. PREVIOUS WORK

In general, the primary data sets used in most building extraction systems are images and DSM, which are used separately or simultaneously. Brunn and Weidner (1998) segmented DSM for building extraction. However it is difficult to apply this algorithm to DSM derived from LIDAR data due to noisy outliers. After that, many building extraction method from LIDAR data were suggested (Morgan and Tempfli, 2000; Priestnall et al., 2000; Wang and Schenk, 2000; Alharthy and Bethel, 2002), however, the building extraction results using DSM still suffer from outliers and relatively low resolution.

There are many efforts to use aerial or satellite images as the single data source for building extraction by means of auxiliary information such as shadow (Lin and Nevatia, 1998), perceptual grouping based on the line segment from edge detection (Kim and Muller, 1999; Sohn and Dowman, 2001) or both of them (Wei et al, 2004). However, auxiliary information is not always available, reliable, and precisely co-registered. The building extraction quality varies depending on accuracy of extracted edges and lines.

Multiple images are also widely used to solve the occlusion problem and to use the elevation information by photogrammetric techniques. Roux and McKeown (1994) used a pair of images for building extraction. Noronha and Nevatia (2001) extracted rectangular buildings by hierarchical perceptual grouping and matching. Elaksher et. al. (2003) suggested 3D building extraction using a robust multi-image line-matching algorithm. Oriot (2003) proposed a semi-automatic approach using statistical snakes with disparity map as initials to delineate building edges.

Some other studies used image information combined with elevation information for building extraction (Haala and Hahn, 1995; Zhao and Trinder, 2000; Seresht and Azizi, 2000). Recently, Khoshelham (2005) integrated image and height data

for parametric building reconstruction through interactive refinement. Several recent studies have used color information (Lari and Ebadi, 2007) and the spectral reflectance values to extract the buildings (Lee et al., 2003). Liu et al. (2005) fused high-resolution panchromatic image with low-resolution multi-spectral imagery to use enhanced color and texture information for building extraction.

3. METHODOLOGY

The proposed framework for building extraction consists of the following steps. First, the original RGB color image is converted into CIE $L^* a^* b^*$ image and then the anisotropic diffusion is applied to each $L^* a^* b^*$ image band so that the color information of the objects are enhanced. Second, we generate the J-image that measures the local image inhomogeneities where high pixel values correspond to potential building boundary location and low pixel values correspond to homogeneous region. A J-image is computed from a class map generated by the k-means clustering using the two chromatic bands, a^* and b^*. Based on this J-image, borders between building and background are delineated by the edge-flow based active contour. In the third step, image segmentation is performed to determine building roof compositional polygons. The extracted building region is classified again using k-means clustering with all three bands and then a J-image is generated. With this J-image, image corresponding to a building is segmented by JSEG. From this segmentation result, building roof compositional polygons are segmented. Finally, segmentation result is refined by removing small segments and merging over-segmented ones. As the final result, building roof wireframes are reconstructed.

3.1 Color Space Conversion and Anisotropic Diffusion

Color space conversion. Several color spaces are currently used. The most common one for digital imagery is the RGB space, which represents color by its red, green and blue components. However, the RGB space does not show similarity with human visual system for color perception. In other saying, the differences among colors perceived by human visual system as being of the same entity are not mirrored by similar distances between the points representing those colors in RGB space. This problem can be solved by a uniform color space, e.g., the most widely used one is CIE $L^* a^* b^*$ space. Briefly, CIE $L^* a^* b^*$ space has three major properties: separation of achromatic information from chromatic information, uniform color space, and similarity to human visual system. Due to these properties, this study chooses CIE $L^* a^* b^*$ colors converted from original RGB image for image segmentation. In CIE $L^* a^* b^*$ space, L* represents the luminance component, while a^* and b^* represent color components. The Euclidean distance ΔE between two colors, ($L1^* a1^* b1^*$) and ($L2^* a2^* b2^*$) in CIE $L^* a^* b^*$ space is defined as

$$\Delta E = \sqrt{(L_1^* - L_2^*)^2 + (a_1^* - a_2^*)^2 + (b_1^* - b_2^*)^2}. \quad (1)$$

It is approximately equivalent to the perceptual difference between two colors in human visual system. Based on this uniformity, color image segmentation can be performed by integrating information extracted from each of the three bands. In this study, the original RGB image is converted into CIE $L^* a^* b^*$ image as shown in Figure 1 and the entire processing for building extraction is performed in CIE $L^* a^* b^*$ space.

Anisotropic diffusion. After color space conversion, anisotropic diffusion is applied into image to decrease noise and enhance color information. This is necessary since most real images are noisy and have corrupted data. Anisotropic diffusion is a popular technique for smoothing images while preserving the edges. In addition, color texture sometimes causes erroneous results although color texture provides an important cue for image segmentation. This undesired influence of color texture can be considerably reduced by anisotropic diffusion. Koenderink (1984) pointed out the solution of the heat conduction equation of image I given by equation (2)

$$I_t(x,y,t) = \Delta I(x,y,t) \quad (2)$$

is equivalent to the Gaussian smoothing function when the original image is used as the initial condition, where x and y denote image coordinates and Δ does Laplacian, and t is time. Based on this, Perona and Malik (1990) proposed the anisotropic diffusion to restrain the diffusing not across the boundary. They perform this selective smoothing based on the observation that the magnitude of the first derivative of the image in equation (3) can be used as the conduction coefficient.

$$\nabla I = \sqrt{(\partial I/\partial x)^2 + (\partial I/\partial y)^2} \quad (3)$$

As a result of combining equation (2) and equation (3), the edge-preserving diffusion is formulated as equation (4) where $\breve{g}(\cdot)$ is a nonnegative monotonically decreasing function with $\breve{g}(0) = 1$, and div is divergence.

$$I_t(x,y,t) = div\left(\breve{g}\left(|\nabla I(x,y,t)| \right) \nabla I(x,y,t) \right) \quad (4)$$

Equation (4) blurred original image inversely proportional to the magnitudue of first derivative of the image. Hence, in the result iamge low frequency region is more diffused while high frequency region is less diffused. As a result of this anisotopic diffusion, we can reduce the undesired noise with preserving feature boundary edges. In this study, the anisotropic diffusion of each band is separately performed by solving equation (4) with the level set method. The bottom row of Figure 1 shows an example of color space conversion and anisotropic diffusion.

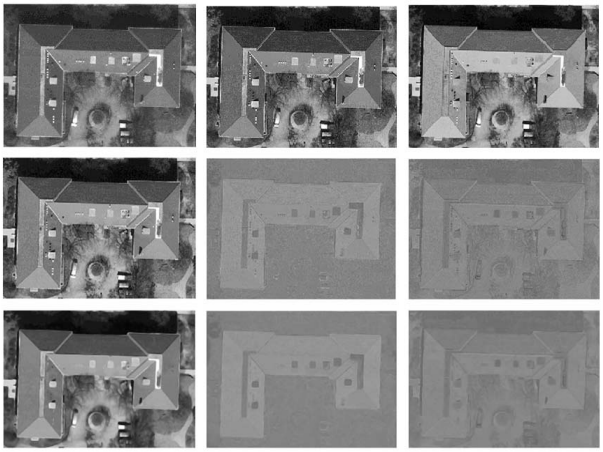

Figure 1. Color space conversion from RGB space to CIE $L^* a^* b^*$ space and the anisotropic diffusion [top: original RGB image (red, green, blue); middle: converted CIE $L^* a^* b^*$ image (L^*, a^* and b^*); bottom: diffused image (L^*, a^* and b^*)]

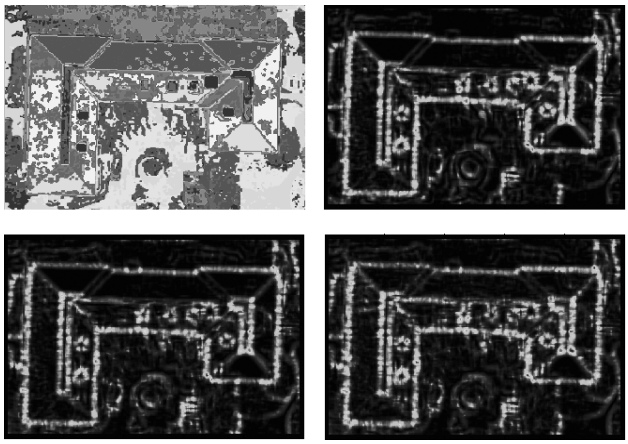

Figure 2. J-images computed with local window [upper: K-means clustering result in CIE a^* b^* domain with 10 clusters, J-image generated from K-means clustering result with 10 clusters; lower: J-1image from K-means clustering result with 15 clusters and 20 clusters]

3.2 Building Boundary Delineation using Active Contour

J-image generation. Image segmentation is based on the local homogeneity of an image, which can be measured by the so-called J-image (Deng et al., 1999). As the prerequisite of J-image computation, we first apply the k-means clustering to the anisotropic diffused image for color quantization. The measure J is then computed based on this class-map as described below. Let Z be the set of all N data points in the class-map, $z=(x,y)$, $z \in Z$. m is the mean as equation (5) and the mean m_i of the N_i data points of class Z_i is defined as equation (6) when Z is classified into C clusters as Z_i, $i=1,2,\cdots,C$.

$$m = \frac{1}{N}\sum_{z \in Z} z \tag{5}$$

$$m_i = \frac{1}{N_i}\sum_{z \in Z_i} z \tag{6}$$

Based on these means, the total distance S_T, the distances S_W within each class and the distances S_B between different classes are determined as below

$$S_T = \sum_{z \in Z} \|z-m\|^2 \tag{7}$$

$$S_W = \sum_{i=1}^{C} S_i = \sum_{i=1}^{C}\sum_{z \in Z_i} \|z-m_i\|^2 \tag{8}$$

$$S_B = S_T - S_W \tag{9}$$

Finally, the measure J is defined as equation (10).

$$J = \frac{S_B}{S_W} = \frac{S_T - S_W}{S_W} \tag{10}$$

The above J value is calculated for each pixel using local window over the entire image. When an image consists of several homogeneous color regions, the color classes from previous clustering are more separated from each other and the value of J becomes larger. In contrast, the value of J becomes smaller when all color classes are more uniformly distributed over the image. The J-image shows higher values around the region boundaries. Figure 2 shows the clustering result (upper left) and J-images which describe the likelihood of a pixel being at the region boundary. In this study, we use the J-image produced from the segmentation result by K-means with 10 clusters. Beside that, Figure 2 presents two more J-images, computed from the k-means clustering using the different cluster numbers of 15 and 20. Visually, these J-images don't show significant differences. From this, we can expect that segmentation using the J-image is not sensitive to the cluster number K unlike the case that K-means is directly used for segmentation.

Edge flow computation. In this study, image segmentation is performed using the active contour, which is deformed towards the edges with high probability to be the segment boundaries by edge flow. Originally, Ma and Majunath (2000) suggested a general framework, named "edge flow", which allows considering different types of image attribute together for image segmentation. The general form of edge flow vector F at image location S with an orientation θ is defined as equation (11)

$$F(s,\theta) = F(E(s,\theta), P(s,\theta), P(s,\theta+\pi)) \tag{11}$$

Where $E(s,\theta)$ is the edge energy at location s along the orientation θ and $P(s,\theta)$ represents the probability of finding the image boundary when the corresponding flow at location s flows in the direction θ, and $P(s,\theta+\pi)$ does the opposite in the direction $\theta+\pi$. The first component is used to measure the energy of local image information change and the remaining two components represent the probability of flow direction. These three components are computed as below. The smoothed image $I_\sigma(x,y)$ is obtained from the original image $I(x,y)$ using the Gaussian kernel $G_\sigma(x,y)$ with a variance σ^2. The prediction error $Err(s,\theta)$ at (x,y) is defined as equation (12) to estimate the probability of finding the nearest boundary in two possible flow directions: the forward and the backward, where d is the prediction distance normalized to the scale σ.

$$Err(s,\theta) = \left| I_\sigma(x + d\cos\theta, y + d\sin\theta) - I_\sigma(x,y) \right| \tag{12}$$

A larger prediction error $Err(s,q)$ in a certain direction implies a higher probability of finding a boundary in that direction. For that reason, the probabilities of edge flow direction are assigned in proportion to their corresponding prediction errors. An edge likelihood $P(s,\theta)$ using relative error is defined as equation (13) and the probable edge direction is then estimated as equation (14).

$$P(s,\theta) = \frac{Err(s,\theta)}{Err(s,\theta) + Err(s,\theta+\pi)} \tag{13}$$

$$\theta' = \arg\max_{\theta} \int_{\theta-\pi/2}^{\theta+\pi/2} P(s,\theta')\,d\theta' \tag{14}$$

The edge flow energy $E(s,\theta)$ at scale σ is defined to be the magnitude of the gradient of the smoothed image $I_\sigma(x,y)$ along the orientation θ as equation (15) when $s=(x,y)$, and n respectively represents the unit vector in the gradient direction.

$$E(s,\theta) = \left|\frac{\partial}{\partial n} I_\sigma(x,y)\right| = \left|I(x,y) * \frac{\partial}{\partial n} G_\sigma(x,y)\right| = \left|I(x,y) * GD_{\sigma,\theta}(x,y)\right| \quad (15)$$

Here, $GD_\sigma(x,y)$ represents the first derivative of the Gaussian along the x-axis so that $GD_{\sigma,\theta}(x,y)$ is the first derivative of the Gaussian along orientation θ and computed as equation (16).

$$GD_{\sigma,\theta}(x,y) = GD_\sigma(x',y') \quad (16)$$

where $\begin{bmatrix} x' \\ y' \end{bmatrix} = \begin{bmatrix} \cos\theta & \sin\theta \\ -\sin\theta & \cos\theta \end{bmatrix} \begin{bmatrix} x \\ y \end{bmatrix}$

Once the flow direction and the edge energy are determined, the "edge flow" field is computed as the vector sum given by

$$\vec{F}(s) = \int_{\theta-\pi/2}^{\theta+\pi/2} [E(s,\theta')\cos\theta' \quad E(s,\theta')\sin\theta']^T \, d\theta' \cdot \quad (17)$$

Once this vector field is produced, the edge flow vectors in the field are propagated towards the edges. This edge flow is respectively computed for L^*, a^* and b^* bands to obtain three edge likelihoods $P_{L^*}(s,\theta)$, $P_{a^*}(s,\theta)$ and $P_{b^*}(s,\theta)$, and three edge energies $E_{L^*}(s,\theta)$, $E_{a^*}(s,\theta)$, and $E_{b^*}(s,\theta)$. The total edge likelihood $P_T(s,\theta)$ and total edge energy $E_T(s,\theta)$ can be computed with equation (18) and (19), respectively

$$P_T(s,\theta) = \left(P_{L^*}(s,\theta) + P_{a^*}(s,\theta) + P_{b^*}(s,\theta)\right)/3 \quad (18)$$

$$E_T(s,\theta) = \sqrt{E_{L^*}(s,\theta)^2 + E_{a^*}(s,\theta)^2 + E_{b^*}(s,\theta)^2} \,. \quad (19)$$

The edge flow from three color-bands is achieved using the total edge likelihood $P_T(s,\theta)$ and total edge energy $E_T(s,\theta)$.

Active contour by level set method: We briefly introduce the active contour before details for image segmentation. Osher and Sethian (1988) suggest level set method to describe the boundary evolution. The development of numerical schemes based on it allows us to handle the topological change of the propagating curve automatically. They represent a curve as a level set of a given function so that the intersection between this function and the coordinate plane yields the curve. Again, the zero level set $\Gamma(t) = \{(x,y) \mid \phi(x,y,t) = 0\}$ of a time-varying surface function $\phi(x,y,t)$, gives the position of boundary at time t. Sethian (1990) suggested curve evolution equation as

$$\phi_t + F\,|\nabla\phi| = 0 \,. \quad \text{given } \phi(x, t=0) \quad (20)$$

In the level set method, the contour curve is evolving by three simultaneous motions through the evolution equation and these three motions are determined by each speed function as

$$F = F_p + F_c + F_a \,. \quad (21)$$

F_p denotes expanding speed with a constant speed F_0 in the normal direction ($F_p = F_0$), F_c moving speed proportional to curvature k when ε is coefficient ($F_c = -\varepsilon k$), and F_a the speed for moving passively by underlying velocity field $\vec{U}(x,y,t)\cdot\vec{N}$ when $\vec{N} = \nabla\phi/|\nabla\phi|$ ($F_a = \vec{U}(x,y,t)\cdot\vec{N}$). By plugging this speed function and rearranging the terms the level set equation can be written as

$$\phi_t + F_0\,|\nabla\phi| + \vec{U}(x,y,t)\cdot\nabla\phi = -\varepsilon k\,|\nabla\phi| \,. \quad (22)$$

The first term after the time derivative on the left is concerned with the propagation expansion speed. This should be approximated through the entropy satisfying schemes. The second term is done with the advection speed. Simple upwind scheme can approximate it through checking the appropriate direction. The third term is curvature speed. This term is like a non-linear heat equation and information propagates in both directions. Hence, an appropriate approach is to use the central difference approximation.

Active contour based image segmentation. This section will explain the image segmentation using active contour based on the J-image and edge flow. We use the edge flow vector field as the external force to enforce the initial contour move towards edges and the measure J as the stopping function instead of the traditional gradient edge penalty function. The initial contour required for active contour is manually achieved under the assumption that approximate foot prints of the buildings can be retrieved from the segmentation result using DSM or multi-spectral images as aforementioned. The contour curve evolution suggested can be formulated

$$C_t = (\vec{S}\cdot\vec{N})\vec{N} + k\breve{J}\vec{N} - F_0\breve{J}\vec{N} \quad (23)$$

where $\vec{S}$ is the edge flow vector field and $\vec{N} = \nabla\phi/|\nabla\phi|$. The stopping function $\breve{J}$ is computed from the J-image as equation (24) through normalization

$$\breve{J}(x,y) = \frac{1}{(1+J(x,y))^2} \quad (24)$$

Accordingly we achieve the level set formulation of the edge flow driven active contour as equation (25)

$$\phi_t - \left(\nabla\cdot\left(\frac{\nabla\phi}{|\nabla\phi|}\right) + F_0\right)\breve{J}(x,y)\,|\nabla\phi| - \vec{S}\cdot\nabla\phi = 0 \quad (25)$$

Figure 3. Building boundary extraction using active contour (upper: Initial boundary, boundary evolution result with 21x21 window; lower; result with 11x11 window, result with 3x3 window as final building extraction)

This active contour is applied to extract the building with multi-scale approach. As aforementioned, the J-image generation and edge-flow computation need a local window. We start active contour evolution with the coarsest J-image and edge-flow generated by the largest window. After that, the evolution is repeated with a finer J-image and edge-flow generated by a smaller window using the previous results as initial. It is iterated until evolution is finished in the finest resolution. Figure 3 shows extracted individual building boundaries by this multi-scale approach using active contour. On the other hand, Figure 4 presents the building extraction when multiple buildings belong to one initial contour. It shows that the proposed active contour can handle the topological change during the evolution. One initial building boundary is divided to three boundaries respectively for three buildings.

Figure 4. Boundary extraction of multiple buildings [upper: Initial boundary (yellow), lower: boundary evolution (red) and extracted boundaries (yellow)]

3.3 Building Roof Polygon Extraction

J-image regeneration. After determine the building boundary, the extracted building region is reclassified by k-means clustering with all three bands, L^*, a^* and b^* and then a J-image is generated from this reclassification result. Figure 5 presents an example of classification result and the J-image based on it.

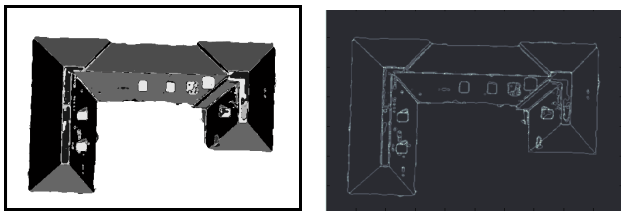

Figure 5. K-means clustering result and the J-image

JSEG for roof polygon segmentation. JSEG is an automatic color image segmentation algorithm proposed by Deng et al. (1999). JSEG consists of two steps: J-image generation and region growing segmentation. This paper performs JSEG segmentation to extract the building roof polygons by simply applying watershed segmentation algorithm (Beucher, 1991) into the J-image. In topography the concepts of watershed and catchment basin are well known. As mentioned before, the J-image is a gray scale image containing high values around the regions expected to be boundaries. Hence the J-image may be interpreted as a topographic surface where the image gray-levels represent elevations. Thus, edges of roof polygons correspond to high watersheds and low-gradient region interiors correspond to catchment basins. After this segmentation, we perform the refinement by merging and removing segments according to the following criteria.

1. A segment entirely surrounded by another segment is merged into the surrounding segment.
2. A segment that is adjacent to background and smaller than 5% of the extracted building region, is removed.
3. The segment adjacent to several segments and smaller than 5% of the extracted building region is merged to the closest segment in terms of the Euclidean distance in CIE $L^* a^* b^*$ space as equation (1)

The first criterion aims at removing small objects such as chimney or window, which are not directly related with the structure frames of building. The purpose of second criteria is to remove the small object adjacent to the main building, for instance air duct, isles, or gate roof. The last criterion attempts to reduce the over segmentation errors due to shade or shadow. The final roof segmentation results and roof wireframe from segmentation result are shown in Figure 6.

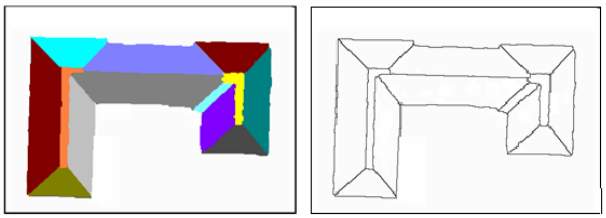

Figure 6. Extracted roof compositional polygons and the reconstructed roof wireframe

4. IMPLEMENTATION AND RESULTS

The data used to examine the proposed framework is an aerial color image of West Lafayette city cropped from Indiana state-wide photography dataset taken in 2005. The image resolution is 15.24 cm. Figure 7 shows the results of several examples. Left images are the original input images and right images show resultant wireframes superimposed on building images. Note that even the building boundary is noisy, the proposed edge-flow driven active contour approach successfully locates the correct building boundary. Also it yields reliable wireframes of building roofs. However, the determined roof compositional polygons are incomplete in some cases. The last result in figure 7 shows over-delineation of building roof due to over-segmentation and loses several details because of under-segmentation.

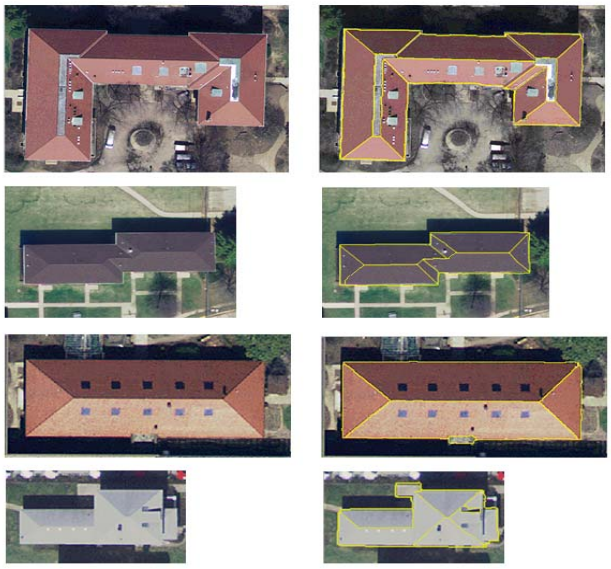

Figure 7. Building extraction results [left: building images; right: extracted roof wireframes]

5. CONCLUSIONS

In this paper, we present a framework to extract buildings from high resolution color imagery. The boundary of a building is delineated by active contour algorithm based on the level set method. For this active contour, the edge flow vector field as external force to enforce contour move towards the edges and the J-image as stopping function instead of the traditional gradient edge penalty function. This shows reliable extraction performance through implementation. Also, the JSEG algorithm is applied to segment the building roof polygons for producing building roof wireframes. The framework demonstrates good and satisfactory results in some cases but the result is not consistent. Because the performance of proposed method depends on the intensity and color information in the image, adjacent roof facades which have the same reflectance values due to the same incident angles to the sunlight can not be separated. This also leads to the need of additional information such as DSM to be incorporated to the proposed algorithm.

REFERENCES

Alharthy, A. and Bethel, J., 2002. Heuristic filtering and 3d feature extraction from LIDAR data. ISPRS The International Archieves of the Photogrammetry, Remote Sensing and Spatial Information Sciences Vol. XXXIV

Brunn, A. and Weidner, U., 1998. Hierarchical Bayesian nets for building extraction using dense digital surface models. ISPRS Journal of Photogrammetry & Remote Sensing, 53(5), pp. 296–307.

Beucher. S., 1991. The watershed transformation applied to image segmentation. Conference on Signal and Image Processing in Microscopy and Microanalysis, pp. 299-314

Deng, Y., Manjunath, B., and Shin, H., 1999. Color image segmentation, Proceedings of the IEEE Computer Society Conference on Computer Vision and Pattern Recognition

Elaksher, F. A., Bethel, S. J., and Mikhail, M. E. , 2003. Roof Boundary Extraction using Multiple Images, Photogrammetric Record, 18(101) , pp. 27-40

Haala, N. and Hahn, M., 1995. Data Fusion for the Detection and Reconstruction of Buildings, In A Gruen, O. Kuebler, P. Agouris (eds), Automatic Extraction of Man-Maid Objects from Aerial and Space Images: 211-220.

Khoshelham, K, 2005. Region Refinement and Parametric Reconstruction of Building Roofs by Integration of Image and Height Data, in Stilla U, Rottensteiner, F. and Hinz, S. (Eds) CMRT05, IAPRS, Vol XXXVI

Kim, T. and Muller, J-P. , 1999. Development of a graph-based approach for building detection, Image and Vision Computing, 17, pp. 3-14

Koenderink, J. J., 1984. The structure of images, Biological Cybernetics, 50, pp. 363-370.

Lari, Z. and Ebadi, H., 2007. Automatic extraction of building features from high resolution satellite images using artificial neural networks, Proceeding of ISPRS conference on Information Extracting from SAR and Optical Data with Emphasis on Developing Countries, Istanbul, Turkey

Lee, S., Shan, J., and Bethel, J. S., 2003. Class-guided building extraction from IKONOS imagery, Photogrammetric Engineering & Remote Sensing, 69(2) , pp. 143-150;

Lin, C. and Nevatia, R., 1998. Building Detection and Description from a Single Intensity Image, Computer Vision and Image Understanding, 72(2), pp. 101-121

Liu, Z. J., Wang, J. and Liu, W.P., 2005. Building Extraction form High Resolution Imagery based on Multi-scale Object Oriented Classification and Probabilistic Hough Transform, Proceedings of the IGARSS 2005, Seoul, Korea

Morgan, M. and Tempfli, K., 2000. Automatic building extraction from airborne laser scanning data, International Archives of Photogrammetry and Remote Sensing, 33(B3/2) , pp. 616–623.

Noronha, S. and Nevatia, R. ,2001. Detection and modeling of buildings from multiple aerial images, IEEE Transactions on Pattern Analysis and Machine Intelligence, 23(5) , pp.501–518,

Oriot, H. ,2003, Statistical snakes for building extraction from stereoscopic aerial images, ISPRS Archives vol XXXIV part 3, pp .65-70

Osher, S. A. and J. A. Sethian, 1988. Fronts Propagating with Curvature Dependent Speed: Algorithms based on Hamilton-Jacobi Formulation, *Journal of Computational Physics*, 79, pp. 12-49

Perona, P. and Malik, J., 1990, Scale-Space and Edge Detection Using Anisotropic Diffusion, IEEE Transactions on Pattern Analysis and Machine Intelligence. 12(7) , pp. 329-639

Priestnall, G., Jaafar, J. and Duncan, A., 2000. Extracting urban features from LIDAR digital surface models. Computers, Environment and Urban Systems, 24, pp. 65-78.

Roux, M. and McKeown, D. M., 1994. Feature matching for building extraction from multiple views. IEEE Proceeding of Computer Vision and Pattern Recognition, pp. 46–53.

Seresht M. and Azizi A., 2000. Automatic Building Recognition from Digital Aerial Images, Proceeding of the 19th ISPRS Congress, Book 3B, pages, pp. 792-798, Amsterdam.

Sethian, J. A., 1990. A Review of Recent Numerical Algorithms for Hyper-surfaces Moving with Curvature Dependent Speed, *Journal of Differential Geometry*, 33, pp.131-161

Sohn, G., and Dowman, I. J., 2001. "Extraction of buildings from high resolution satellite data", In: Balisavias, et al. (Eds), Automatic Extraction of Man-Made Objects from Aerial and Space Images (III),Zurich, 2001.

W. Y. Ma and Manjunath, B. S., 1997. Edge flow: a framework of boundary detection and image segmentation. In Proc. IEEE Conf. on Computer Vision and Pattern Recognition, pp. 744-749

Wang, Z. and Schenk, T., 2000. Building Extraction and Reconstruction from LIDAR Data. International Archives of Photogrammetry and Remote Sensing, 33(B3), pp. 958-964.

Wei, Y., Zhao, Z., and Song, J., 2004 , Urban building extraction from high-resolution satellite panchromatic image using clustering and edge detection, IEEE Proceeding of IGARSS 2004, 3, pp. 2008-2010

Zhao, B. and Trinder J., 2000, Integrated Approach Based Automatic Building Extraction. Proceeding of the 19th ISPRS Congress, Amsterdam Book 3B, pp. 1026-1032